SUPPORTING INFORMATION FOR

Unexpected Molecular Sieving Properties of Zeolitic Imidazolate Framework-8

Chen Zhang[†], Ryan P. Lively[‡], Ke Zhang[†], Justin R. Johnson[†], Oguz Karvan[†], William J. Koros*[,†]

[†]*School of Chemical & Biomolecular Engineering, Georgia Institute of Technology, 311 Ferst Dr. NW, Atlanta, Georgia 30332-0100, United States*

[‡]*Algenol Biofuels, 28100 Bonita Grande Dr., Bonita Springs, FL 34315, United States*

* E-mail address: wjk@chbe.gatech.edu

Section S1: Synthesis of ZIF-8 nano- and microcrystals

Materials

All chemicals were purchased from Sigma-Aldrich and used as received without further purifications.

Chemical	Purity
$Zn(NO_3)_2 \cdot 6H_2O$	≥99.0%
2-methylimidazole	99.0%
sodium formate	≥99.0%
methanol, anhydrous	99.8%

Synthesis of 26 nm ZIF-8 crystals

The 26 nm ZIF-8 crystals were synthesized using the procedure reported by Cravillon and co-workers[1]. 588 mg (1.977 mmol) $Zn(NO_3)_2 \cdot 6H_2O$ and 811mg (9.883 mmol) 2-methylimidazole were each dissolved in 40 ml methanol. The molar ratio of Zn/MeIM/MeOH was 1:5:1000. The latter solution was poured into the former solution under stirring with a magnetic bar. Stirring was stopped after 7 min, and then the white solids were separated from the milky colloidal dispersion by centrifugation, followed by extensive washing with methanol. The product was dried at room temperature under vacuum.

Synthesis of 7.9 μm ZIF-8 crystals

The 7.9 μm ZIF-8 crystals were synthesized by modifying the procedure reported by Cravillon and co-workers[2]. 588 mg (1.977 mmol) $Zn(NO_3)_2 \cdot 6H_2O$ was dissolved in 40 ml methanol. 324 mg (3.954 mmol) 2-methylimidazole and 538 mg (7.908 mmol) sodium formate were dissolved in 40 ml methanol. The molar ratio of Zn/MeIM/$NaHCO_2$/MeOH was 1:2:4:1000. The latter solution was poured into the former solution under stirring with a magnetic bar. Stirring was stopped upon mixing. The solution was heated at 90℃ for 24 hours in a sealed glass jar. The crystals were recovered by

centrifugation, followed by extensive washing with methanol. The product was dried at room temperature under vacuum.

Synthesis of 162 μm ZIF-8 crystals

The 162 μm ZIF-8 crystals were synthesized by modifying the procedure reported by Cravillon and co-workers[2]. 3.528 g (11.862 mmol) $Zn(NO_3)_2 \cdot 6H_2O$ was dissolved in 40 ml methanol. 1.944 g (23.724 mmol) 2-methylimidazole and 0.807 g (11.862 mmol) sodium formate were dissolved in 40 ml methanol. The molar ratio of Zn/MeIM/$NaHCO_2$/MeOH was 1:2:1:166.5. The latter solution was poured into the former solution under stirring with a magnetic bar. Stirring was stopped upon mixing. The solution was heated at 90℃ for 24 hours in a sealed glass jar. The large crystals on the wall of the jar were collected and washed extensively with methanol. The product was dried at room temperature under vacuum.

Section S2: Characterization of ZIF-8 nano- and microcrystals

Scanning Electron Microscope (SEM)

SEM images (Figure 1) of synthesized ZIF-8 nano- and microcrystals as well as the BASF ZIF-8 crystals were obtained on a LEO 1530 field emission scanning electron microscope (LEO Electron Microscopy, Cambridge, UK).

Powder x-ray diffraction (PXRD)

PXRD data were collected on a Phillips X'Pert X-Ray Diffractometer (using Cu Kα radiation, λ=0.154 nm at 45kV and 40 mA). Experiments were carried out scanning from 2θ =5-40°. PXRD patterns of the synthesized ZIF-8 samples match well with the simulated one.

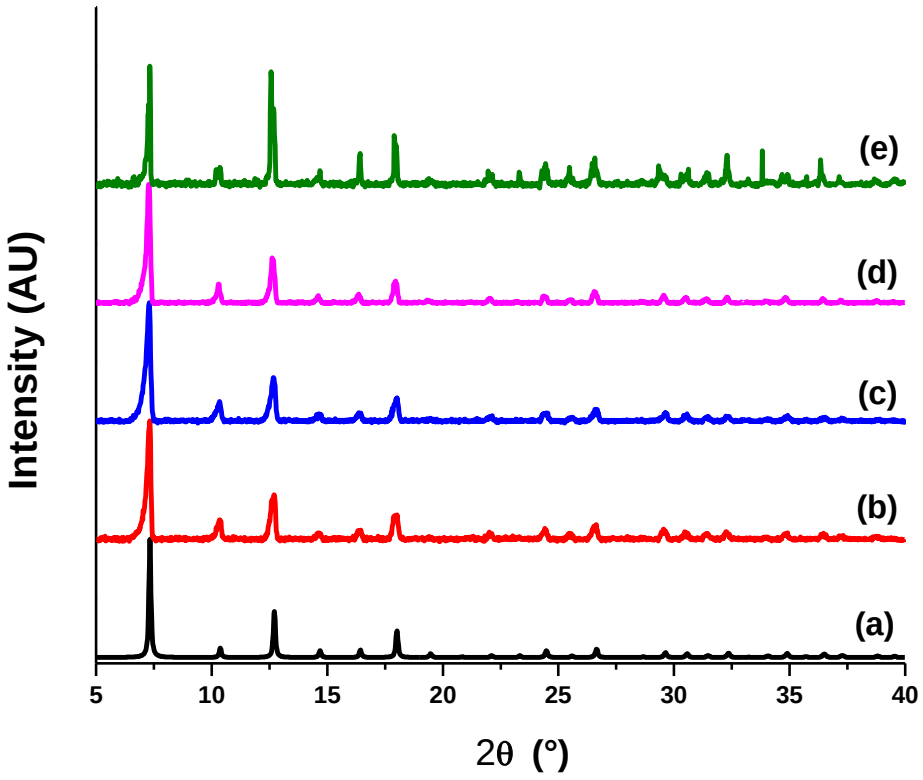

Figure S1. PXRD patterns of ZIF-8 (a) simulated (b) 200 nm BASF sample (c) 26 nm synthesized sample (d) 7.9 μm synthesized sample (e) 162 μm synthesized sample

Thermogravimetric analysis (TGA)

Samples were activated in a vacuum oven at 150 ℃ for 12 hours prior to analysis in a Netzsch STA 409 TGA instrument. Samples were heated to 800 ℃ with a constant heating rate of 10℃/min in an air atmosphere. As shown in Figure S2, the total percentage mass change (64.1-64.5%) after decomposition agree well with the percentage mass change (64.6%) calculated by the molecular weight of $Zn(MeIM)_2$, assuming that ZnO was the only solid after decomposition and oxidation.

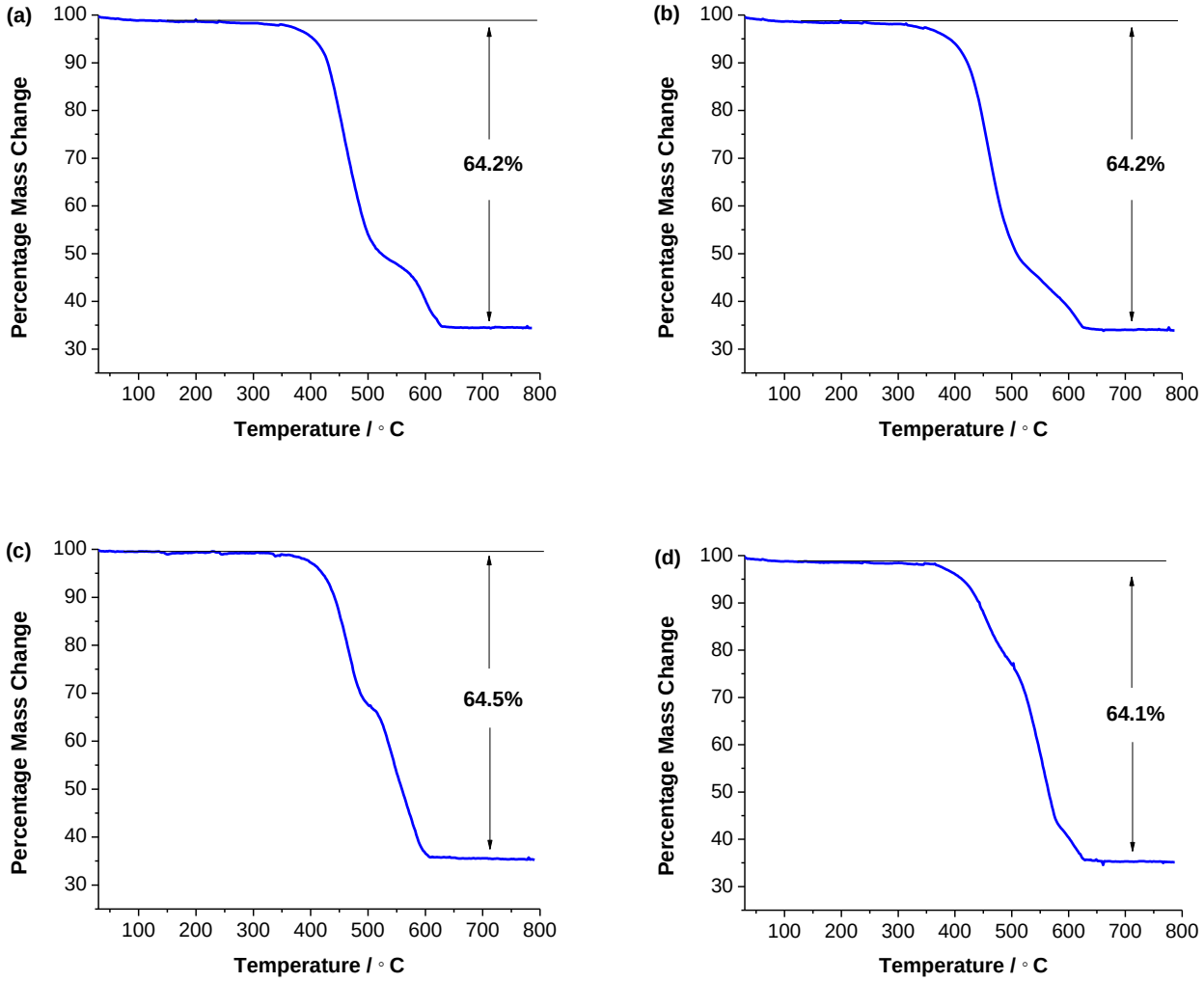

Figure S2. TGA curves of ZIF-8 (a) 200 nm BASF sample (b) 26 nm synthesized sample (c) 7.9 μm synthesized sample (d) 162 μm synthesized sample.

Crystal size analysis

Crystal size distribution and average crystal size of the 26 nm ZIF-8 sample were analyzed with a Protein Solutions DynaPro dynamic light scattering (DLS) device. The distribution shown in Figure S3 (a) was an average of 20 scans. The crystal size distribution and average crystal size of 7.9 μm and 162 μm ZIF-8 samples were obtained by each randomly analyzing ~200 crystals using a Nikon Eclipse 50i microscope. Since crystals were randomly selected for size analysis, we believe that the crystal size distributions shown in Figure S3 (b) & (c) are representative of both samples. For (truncated) rhombic dodecahedron shaped crystals, the equivalent spherical crystal radius was taken to be the radius of a sphere with equivalent volume. For crystals with less regular shapes, the equivalent spherical crystal radius was taken to be the radius of the smallest circle that can encompass the entire crystal under the microscope.

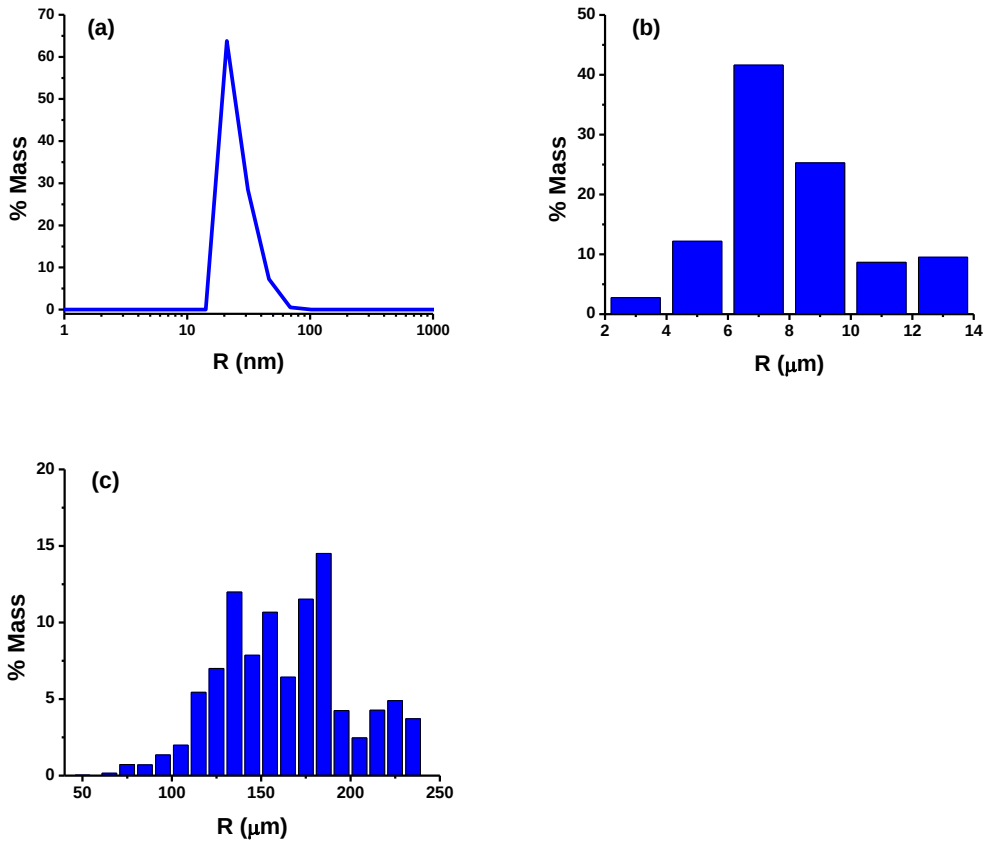

Figure S3. Crystal size distributions of (a) 26 nm ZIF-8 sample (b) 7.9 μm ZIF-8 sample (c) 162 μm ZIF-8 sample.

The average equivalent spherical crystal radius of the 7.9 μm and 162 μm ZIF-8 sample was then calculated by:

$$\bar{R} = \frac{\sum_i V_i R_i}{\sum_i V_i} = \sum_i X_i R_i \qquad (1)$$

where R_i and V_i are the equivalent spherical crystal radius and volume of each individual crystal, X_i is the volume/weight fraction of crystals with a radius of R_i. As will be shown later, the crystal size distributions illustrated in Figure S3 were used to estimate effective diffusivities in ZIF-8.

N_2 physisorption at 77K

The microporous structure of synthesized ZIF-8 samples was confirmed after observation of Type I N_2 physisorption isotherms at 77K (Figure S4), which were obtained using an ASAP 2020 instrument. Samples were activated at 150℃ for 16 hours prior to adsorption measurements. Surface areas calculated using the Brunauer-Emmett-Teller (BET) and Langmuir model are tabulated in Table S1. The BET surface areas of synthesized ZIF-8 samples were in the range of 1560~1621 m^2/g, which were higher than the BASF ZIF-8 sample and close to the value (1630 m^2/g) reported for ZIF-8 microcrystals[3]. The measured surface areas were also in agreement with the value estimated using single crystal XRD results[3]. The surface area of the 26 nm ZIF-8 sample is considerably higher than the reported surface area of a ZIF-8 nano-crystal sample synthesized using the same procedure[1].

As shown in Figure S4, the adsorption step above relative pressure p/p_0=0.9 increases with decreasing crystal size, which is a result of increasing external surface area. A careful look at the log-linear plot of the N_2 physisorption isotherm below p/p_0=0.1 reveals the existence of two sub-steps, which were previously observed on ZIF-8 and siliceous MFI zeolites and were believed to be the result of phase transitions of the adsorbed N_2 molecules[3,4]. However, recent work on ZIF-8 N_2 physisorption indicates that this step could also be the result of guest-induced framework rearrangement[5]. The underlying cause of this step has yet to be definitively resolved.

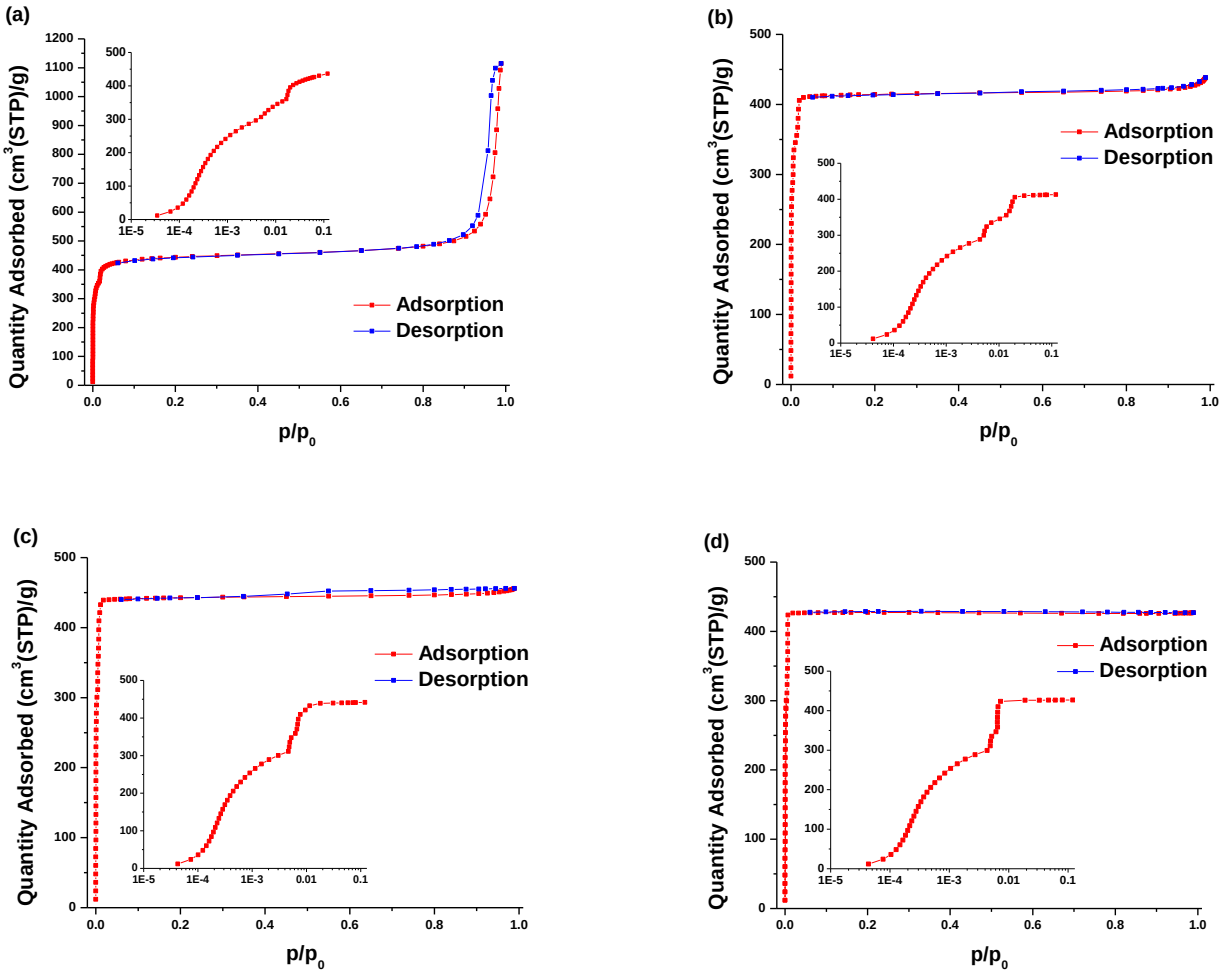

Figure S4. N_2 physisorption isotherm at 77K (a) 26 nm synthesized ZIF-8 sample (b) 200 nm BASF sample (c) 7.9 μm synthesized ZIF-8 sample (d) 162 μm synthesized ZIF-8 sample. Red and blue dots correspond to adsorption and desorption processes, respectively.

Table S1. BET and Langmuir surface areas based on N_2 physisorption at 77K

Sample	BET S_A (m^2/g)	Langmuir S_A (m^2/g)
26nm	1615±13	1927±7
BASF (200nm)	1517±15	1814±3
7.9 μm	1621±15	1937±3
162 μm	1560±15	1871±3

Section S3: Calculation of diffusivities from kinetic uptake rate measurements

Gas and vapor adsorption isotherms on ZIF-8 at 35 ℃

Adsorption isotherms and kinetics of the studied gases were obtained using the pressure decay method[6], in which the amount adsorbed and the rate of adsorption were measured by monitoring the decreasing pressure of the sample chamber with a fixed volume. On the other hand, adsorption isotherms and kinetics of ethanol vapor were obtained using the gravimetric method, in which the amount adsorbed and adsorption rates were measured by monitoring the sample weight to avoid problems with sorption on cell walls. Details of the employed pressure decay and gravimetric methods will be shown later.

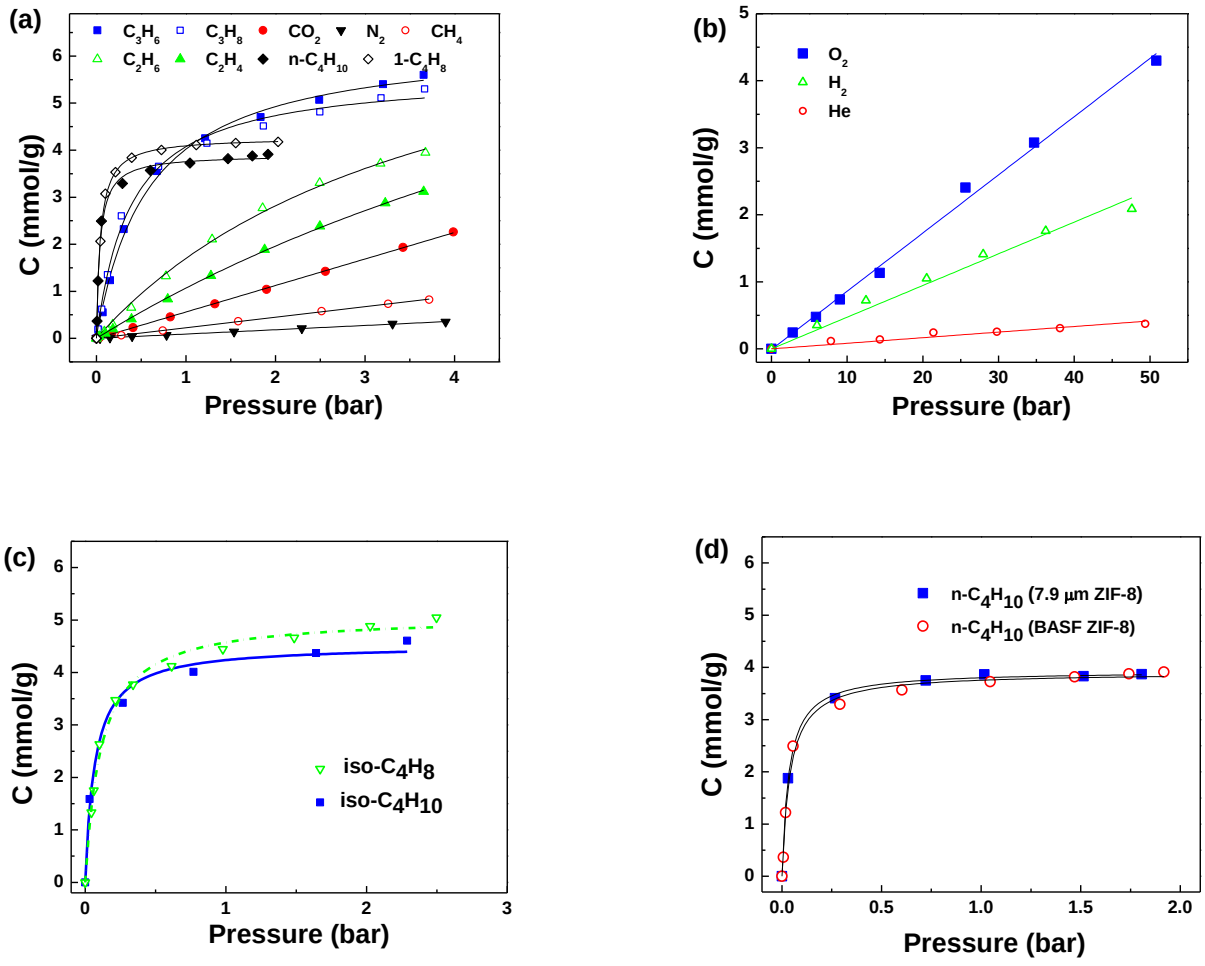

Figure S5. (a) & (b) Adsorption isotherms on the BASF ZIF-8 sample at 35 ℃. (c) Adsorption isotherms of iso-C_4H_8 and iso-C_4H_{10} on the 26 nm synthesized ZIF-8 sample at 35 ℃. (d) Adsorption isotherms of n-C_4H_{10} on the BASF ZIF-8 and 7.9 μm synthesized ZIF-8 samples at 35 ℃.

The adsorption isotherms of CO_2, N_2, CH_4, C_2H_4, C_2H_6, C_3H_6, C_3H_8, 1-C_4H_8 and n-C_4H_{10} in ZIF-8 were obtained using the 200 nm BASF ZIF-8 sample at 35 ℃ up to 4 bars, as shown in Figure S5 (a). The adsorption isotherms of He, H_2, and O_2 were obtained using the same ZIF-8 sample at 35 ℃ up to 50 bars, as shown in Figure S5 (b). The adsorption isotherms of iso-C_4H_8 and iso-C_4H_{10} were measured on the 26 nm synthesized ZIF-8 sample with much faster uptake, as shown in Figure S5 (c). The adsorption isotherm of n-C_4H_{10} was measured on both the BASF ZIF-8 and 7.9 μm synthesized ZIF-8 samples and illustrated in Figure S5 (d), showing almost identical adsorption capacities.

The adsorption isotherms of above mentioned gases with the exception of He, H_2, CO_2, O_2, N_2, and CH_4 in ZIF-8 at 35 ℃ were fit using the Langmuir model:

$$C(p) = \frac{C_s bp}{1 + bp} \tag{2}$$

where p is gas-phase equilibrium pressure (bar), $C(p)$ is the amount adsorbed (mmol/g), C_s is the capacity constant (mmol/g), and b is the affinity constant (1/bar). In the pressure range where the product of affinity constant and equilibrium pressure is negligible compared with unity, the Langmuir model can be reduced to the Henry's law:

$$C(p) \approx C_s bp = Kp \tag{3}$$

$$(K = C_s \times b)$$

where K is the Henry's constant, mmol/(g bar). The adsorption isotherms of He, H_2, CO_2, O_2, N_2, and CH_4 in ZIF-8 were essentially linear at 35 ℃ in the studied pressure range and hence were fit using the Henry's law. The fitting parameters were tabulated in Table S2.

Table S2. Langmuir model parameters and Henry's constants at 35 ℃

Adsorbate	C_S (mmol/g)	b (1/bar)	K (mmol/(g·bar))	Polarizability[7] (10^{-24} cm^3)
He	N/A	N/A	0.013	0.21
H_2	N/A	N/A	0.039	0.80
CO_2	N/A	N/A	0.563	2.91
O_2	N/A	N/A	0.087	1.58
N_2	N/A	N/A	0.091	1.74
CH_4	N/A	N/A	0.224	2.59
C_2H_4	11.8	0.10	1.18	4.25
C_2H_6	8.25	0.26	2.15	4.47
C_3H_6	6.36	1.72	10.9	6.26
C_3H_8	5.65	2.59	14.6	6.29
1-C_4H_8	4.28	22.4	95.9	8.52
n-C_4H_{10}*	3.91	24.9	97.4	8.20
iso-C_4H_8**	5.08	9.0	45.7	8.29
iso-C_4H_{10}**	4.53	14.6	66.1	8.14

*Fit using the n-C_4H_{10} isotherm on the BASF ZIF-8 sample

** Fit using isotherms on the 26 nm synthesized ZIF-8 sample

At ambient temperature and low surface coverage (Henry's law region), the isosteric heat of adsorption ΔH (J/mol) is related to the interaction potential energy ϕ (J/mol) between adsorbate molecules and the adsorbent surface, which consists of non-electrostatic energies (dispersion energy, close-range repulsion energy, and induction energy) as well as electrostatic energies arising from field-dipole and field gradient-quadrupole interactions[8,9]. For a given adsorbent, the non-electrostatic energies are essentially proportional to the polarizability of adsorbate molecules[9]. Unlike cationic aluminosilicate zeolites (e.g. zeolite A and X) with surface electric charges, the surface of ZIF-8 is non-polar and absent of free charges. Therefore, the interaction potentials in ZIF-8 should be dominated by non-electrostatic energies and the isosteric heats of adsorption in ZIF-8 are expected to be proportional to adsorbate polarizabilities. Unfortunately, equilibrium adsorption data were not available at multiple temperatures in our study, and therefore, the value of ΔH cannot be determined experimentally.

As shown by Figure 3, the logarithm of Henry's constants ($\ln K$) on ZIF-8 at 35℃ is generally linearly correlated to adsorbate polarizabilities. While it does not necessarily indicates the absence of any field-dipole and field gradient-quadrupole interactions, the good correlation strongly suggests that the interaction potentials between the studied adsorbate molecules and ZIF-8 surface are dominated by

non-electrostatic energies. While the quardupole moment of N_2 is almost three times larger than O_2 (-5.0×10^{-40} vs. -1.3×10^{-40} C·m^2)[10], N_2 adsorbs slightly stronger than O_2 on ZIF-8 merely due to its marginally higher polarizability (Table S2).

The ethanol vapor uptake into ZIF-8 (Figure S6, showing similar adsorption capacities of ethanol on the BASF and the 162 μm synthesized ZIF-8 sample) was similar to that observed in ZIF-71[11]. The isotherm is a typical Type IV isotherm, which implies that ethanol forms a monolayer within the cages at low activities, while capillary condensation occurs at higher activities. Recent modeling studies[12] on the ethanol/ZIF-71 system predict the capillary condensation even though a rigid framework model was used, thus likely indicating the "step" in the isotherm is not a result of framework flexibility. While no such modeling study yet exists for ZIF-8, it is reasonable to conclude that a similar phenomenon is taking place.

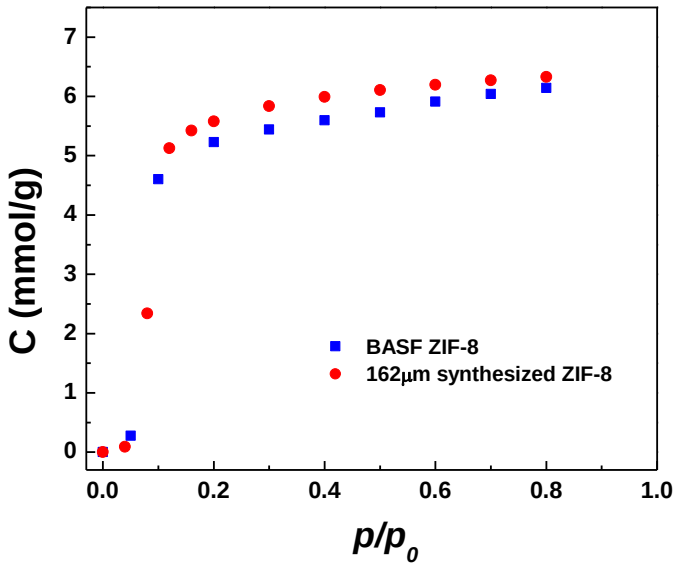

Figure S6. Adsorption isotherms of C_2H_5OH on the BASF and 162 μm synthesized ZIF-8 sample at 35 ℃.

Analysis of gas kinetic uptake data

Thermodynamically corrected diffusivities (D_0) of C_3 and C_4 hydrocarbons in ZIF-8 were obtained using the measured effective transport diffusivities (D_e) with a correction factor taking into

account the loading dependence of the transport diffusivity. The effective transport diffusivities were measured by matching the initial region of the experimental kinetic uptake curves ($0<M_t/M_\infty<0.2$) to the analytical solution of an isothermal transient diffusion model with intracrystalline diffusion control and non-constant boundary concentrations. In our study, kinetic uptake data were available at 35 ℃ only, and therefore activation energies for micropore diffusion cannot be estimated experimentally.

Kinetic uptake rate measurements have been among the oldest and most reliable techniques to estimate transport diffusivities in micropores of microporous materials such as zeolites, carbon molecular sieves, and metal-organic frameworks. The kinetic uptake curve can be obtained by monitoring either the decreasing rate of sample chamber pressure (piezometric) or increasing rate of sample weight (gravimetric) during kinetic adsorption[13].

The illustration of the pressure decay adsorption device employed for gas kinetic uptake measurements can be found elsewhere[6]. The ZIF-8 powder sample was sealed in a 0.5 μm filter element and installed in the sample chamber with a small and fixed volume, which is connected to the reservoir with an automated valve controlled by a computer. The volumes of sample chamber and reservoir were precisely determined. Pressure in the sample chamber and reservoir were each monitored by highly-sensitive pressure transducers. The entire device was placed in a constant temperature (35 ℃) oil bath equipped with a temperature circulator. The sample chamber was initially under vacuum before starting the uptake rate measurements. The gas was first introduced into the reservoir with the automated valve closed. After thermal equilibrium was obtained in the reservoir, the automated valve is opened shortly for one second and then closed. The pressure loss in the sample chamber (which is a result of adsorption by the sample) is monitored by the pressure transducer connected to the sample chamber and recorded by a computer. The initial data points (typically 5~20 seconds) after closing the valve were not used to plot the experimental uptake curve since they were influenced by response of the pressure transducer as well as rapid expansion of gases upon opening of the valve[14]. The sample chamber pressure right after closing the valve (t=0) was calculated by mass balance using the reservoir pressure (after closing the valve) and the known volumes of the sample chamber and reservoir, in order to obtain the entire uptake

curve. ZIF-8 sample was activated at 150 ℃ under vacuum for 10-12 hours and further evacuated in the sample chamber at 35 ℃ under vacuum for another 10-12 hours before uptake measurements.

The transport diffusivity of adsorbate molecules in the micropores of microporous material is dependent on the adsorbate loading in the particle[13]:

$$D = D_0 \frac{d \ln p}{d \ln C(p)} \tag{4}$$

where D (cm^2/s) is the loading-dependent transport diffusivity, D_0 (cm^2/s) is the thermodynamically corrected diffusivity (the Maxwell-Stefan diffusivity[15]), $C(p)$ (mmol/g) is the amount adsorbed, and p (bar) is the gas-phase equilibrium pressure. Therefore, D/D_0 is dependent on the non-linearity of the adsorption isotherm. Generally, assuming that the adsorption isotherm can be described using the Langmuir model (equation S2), it will be easy to obtain the following relationship[13]:

$$D = \frac{D_0}{1-\theta} \tag{5}$$

Where $\theta = C(p)/C_s$, which is the surface fractional coverage.

For less strongly adsorbed species (i.e. He, H_2, CO_2, O_2, N_2, and CH_4, as shown in Figure S5 and Table S2), the isotherm is essentially linear in the studied pressure range and D will be essentially identical to D_0. For more strongly adsorbed species (i.e. C_2H_4, C_2H_6, C_3H_6, C_3H_8, 1-C_4H_8, n-C_4H_{10}, iso-C_4H_8, and iso-C_4H_{10}, as shown in Figure S5 and Table S2), D/D_0 will be non-negligible even at low pressures. Therefore, to study the molecular sieving behavior of ZIF-8, it will be more meaningful to compare the thermodynamically corrected diffusivity D_0 instead of the loading-dependent transport diffusivity D.

Generally, the effective intracrystalline transport diffusivity D_e can be calculated by fitting the experimental kinetic uptake curve ($M_t / M_\infty \sim t^{1/2}$) obtained from kinetic uptake rate measurements with the theoretical uptake curve derived from analytical solution to the model of transient diffusion with intracrystalline diffusion control[16,17]. For *a* spherical particle subject to a step change in adsorbate concentration at its external surface at time zero, the fractional uptake is equal to[18]:

$$\frac{M_t}{M_\infty} = 1 - \frac{6}{\pi}\sum_{n=1}^{\infty}\frac{1}{n^2}\exp(-\frac{n^2\pi^2 Dt}{R^2}) \quad (6)$$

where M_t (mmol) and M_∞ (mmol) are moles adsorbed during time t and as $t \to \infty$, D (cm^2/s) is the transport diffusivity, R (cm) is the equivalent spherical crystal radius of the adsorbent particle. In the short time region, the kinetic uptake curve is essentially linear and approximated by[18]:

$$\frac{M_t}{M_\infty} \approx \frac{6}{\sqrt{\pi}}\sqrt{\frac{Dt}{R^2}} \quad (7)$$

In our study, a collection of crystals with non-uniform crystal sizes (Figure S3) instead of a single crystal were used for adsorption rate measurements. It was suggested by Ruthven and co-workers[16] that it was not possible to obtain reliable intracrystalline diffusivity data using the average equivalent spherical crystal radius if the individual crystal sizes are widely distributed. Instead, their study showed that accurate diffusivities can be determined by taking into account the crystal size distribution. For *a collection of* particles with a size distribution, Equation S6 and S7 can be re-written as:

$$\frac{M_t}{M_\infty} = \sum_i X_i(\frac{M_t}{M_\infty})_i = 1 - \frac{6}{\pi}\sum_i\sum_{n=1}^{\infty} X_i\frac{1}{n^2}\exp(-\frac{n^2\pi^2 Dt}{R_i^2}) \quad (8)$$

$$\frac{M_t}{M_\infty} = \sum_i X_i(\frac{M_t}{M_\infty})_i \approx \frac{6}{\sqrt{\pi}}\sum_i X_i\sqrt{\frac{Dt}{R_i^2}} \quad (9)$$

where X_i is the weight fraction of particles with a radius of R_i (Equation S1 and Figure S3).

The effective transport diffusivity D_e obtained by matching the experimental kinetic uptake curve with Equation S9 will be equal to the corrected diffusivity D_0 provided that (1) the uptake is controlled by intracrystalline diffusion (2) the temperature of the adsorbent particle is constant during the uptake, i.e. isothermal adsorption (3) the adsorbate concentration is constant during the uptake in the ambient of the particle (4) the concentration in the adsorbent particle is sufficiently low and the concentration change is differential.

In our study, pure gases were introduced into the sample chamber without carrier gases and transport is only limited by intracrystalline diffusion in the micropores. For kinetic uptake of the studied

C_3 and C_4 hydrocarbons in the synthesized ZIF-8 samples, the adsorption rate was sufficiently slow (Figure 2) compared to heat dissipation and therefore the assumption of isothermal adsorption should be valid. However, since the adsorption rate was measured by decreasing pressure in the sample chamber, a deviation from the third assumption was inevitable. Hence, instead of using Equation S9 to calculate diffusivities, a modified model taking into account the non-constant boundary concentration was used to calculated transport diffusivity of the studied C_3 and C_4 hydrocarbons in ZIF-8. Moreover, the fourth assumption was not satisfied either. The adsorption isotherm of the strongly adsorbed C_3 and C_4 hydrocarbons are non-linear during the uptake, and therefore the loading dependence was also taken into account for diffusivity calculations, which will be shown later.

In the short time region, the transient diffusion in *a* spherical particle with decreasing adsorbate concentration in the ambient of the particle can be described as[18]:

$$\frac{M_t}{M_\infty} \approx (1+\alpha)\left[1-\frac{\gamma_1}{\gamma_1+\gamma_2}eerfc\left\{\frac{3\gamma_1}{\alpha}\left(\frac{Dt}{R^2}\right)^{1/2}\right\}-\frac{\gamma_2}{\gamma_1+\gamma_2}eerfc\left\{\frac{3\gamma_2}{\alpha}\left(\frac{Dt}{R^2}\right)^{1/2}\right\}\right] \tag{10}$$

$$\alpha = \frac{1}{\Lambda}-1 \tag{11}$$

$$eerfc(z) \equiv \exp(z^2)\times erfc(z) \tag{12}$$

where Λ is the fraction of adsorbate added in the step that is finally adsorbed by the adsorbent particle, and γ_1 and γ_2 are functions of α. Similarly to Equation S7, for *a collection of* particles with a size distribution, Equation S10 can be re-written as:

$$\frac{M_t}{M_\infty} = \sum_i X_i\left(\frac{M_t}{M_\infty}\right)_i \approx \sum_i X_i(1+\alpha)\left[1-\frac{\gamma_1}{\gamma_1+\gamma_2}eerfc\left\{\frac{3\gamma_1}{\alpha}\left(\frac{Dt}{R_i^2}\right)^{1/2}\right\}-\frac{\gamma_2}{\gamma_1+\gamma_2}eerfc\left\{\frac{3\gamma_2}{\alpha}\left(\frac{Dt}{R_i^2}\right)^{1/2}\right\}\right] \tag{13}$$

In our work, effective diffusivities (Table S3) of the studied C_3 and C_4 hydrocarbons were obtained by matching the initial region of the experimental uptake curve ($0<M_t/M_\infty<0.2$) to the theoretical uptake curve derived from equation S13 for a collection of particles with size distribution as shown in Figure S3.

For macroscopic kinetic uptake rate measurements, it is preferred to have differential concentration change during the uptake[13,14]. However, in our study, the size of the concentration step was limited by the sensitivity of the pressure transducer. The studied C_3 and C_4 hydrocarbons adsorb very strongly on ZIF-8 and the isotherms were not linear during the uptake. Therefore, the effective diffusivity D_e obtained previously was an averaged value[17]:

$$\frac{D_e}{D_0} = \frac{5}{3}\frac{1}{(\theta_\infty^{5/3} - \theta_0^{5/3})}\int_{\theta_0}^{\theta_\infty} \theta^{2/3} f(\theta) d\theta \tag{14}$$

where θ_0 and θ_∞ are surface fractional coverage at the beginning and the end of the uptake. If the adsorption isotherm is Langmuir type[17]:

$$\frac{D_e}{D_0} = \frac{5}{U_\infty^5 - U_0^5}\{\frac{1}{6}\ln\left[\frac{(1+U_\infty+U_\infty^2)}{(1-U_\infty)^2}\frac{(1-U_0)^2}{(1+U_0+U_0^2)}\right] - \frac{1}{\sqrt{3}}\tan^{-1}\left(\frac{1+2U_\infty}{\sqrt{3}}\right) + \frac{1}{\sqrt{3}}\tan^{-1}\left(\frac{1+2U_0}{\sqrt{3}}\right) - \frac{U_\infty^2}{2} + \frac{U_0^2}{2}\} \tag{15}$$

Where $U_0 = \theta_0^{1/3}$ and $U_\infty = \theta_\infty^{1/3}$.

The corrected transport diffusivities of the studied C_3 and C_4 hydrocarbons in ZIF-8 are shown in Table S3. D_{ES-7} is the effective transport diffusivity obtained by matching the region of $0<M_t/M_\infty<0.2$ of the uptake curve in Figure 2 with Equation S7, using the average crystal radii $\bar{R}$. D_{ES-13} is the effective transport diffusivity obtained by matching the region ($0<M_t/M_\infty<0.2$) of the uptake curve in Figure 2 with Equation S13. For the studied C_3 and C_4 hydrocarbons, a comparison of D_{ES-7} and D_0 will reveal that neglecting the fact of non-constant boundary concentration and the loading dependence of transport diffusivity will lead to significantly overestimated values.

Table S3. Calculation results of corrected diffusivities of the studied $C_3 \sim C_4$ hydrocarbons and C_2H_5OH in ZIF-8 at 35 ℃ ($\theta_0 = 0$ for all cases).

	$D_{ES\text{-}7}$ (cm^2/s)	$D_{ES\text{-}13}$ (cm^2/s)	Λ	θ_∞	D_e/D_0	D_0 (cm^2/s)
C_3H_6	4.6×10^{-8}	3.3×10^{-8}	0.16	0.18	1.13	2.9×10^{-8}
C_3H_8	3.1×10^{-10}	2.2×10^{-10}	0.213	0.13	1.09	2.0×10^{-10}
1-C_4H_8	1.4×10^{-10}	1.9×10^{-11}	0.66	0.51	1.52	1.3×10^{-11}
n-C_4H_{10}	1.2×10^{-11}	8.0×10^{-12}	0.20	0.43	1.40	5.7×10^{-12}
iso-C_4H_8	3.8×10^{-15}	5.2×10^{-16}	0.65	0.29	1.23	4.2×10^{-16}
iso-C_4H_{10}	4.3×10^{-18}	2.7×10^{-18}	0.15	0.22	1.16	2.3×10^{-18}
C_2H_5OH	1.4×10^{-9}	N/A	N/A	N/A	1.0	1.4×10^{-9}

In Figure 4, diffusivities measured from ZIF-8 samples with significantly different crystal sizes (nano- and microcrystals) were compared, based on the knowledge that Fickian diffusivity is not a function of crystal size. This assumption has been shown to be valid for zeolite 5A with relatively rigid frameworks[19]. On the other hand, it has been suggested that vapor transport in polymers can involve a relaxation process due to swelling of polymer chains in addition to Fickian diffusion. For these systems, the shape of kinetic uptake curves may deviate from Fickian type responses depending on the type of polymer, vapor phase activities, as well as polymer sample sizes, etc.[20-22] The framework of ZIF-8 is locally flexible due to rotation of MeIM ligand[5], however; long-range flexibility does not exist in the ZIF-8 framework that is constructed by covalently bonded Zn and MeIM. Therefore, swelling effects are not expected in ZIF-8 (as demonstrated by Fickian type responses in Figure 2) and the assumption that Fickian diffusivity of a particular adsorbate is irrelevant of sample size should be valid for our study.

Uncertainties of diffusivity data obtained from kinetic uptake rate measurements may arise from approximating the polyhedral microcrystals to be spherical particles. It has been suggested that the crystal shape has negligible effects on the slope of uptake curve in its initial region, as long as the

crystal size is approximated by the equivalent spherical radius[13]. In our study, since diffusivities were obtained from the initial region of the experimental uptake curves, the uncertainties arising from crystal shape should be quite limited.

Analysis of vapor kinetic uptake data

The adsorption equilibria and kinetic uptake rate measurements of C_2H_5OH vapor were performed on a VTI-SA vapor sorption analyzer from TA Instruments (New Castle, DE, United States) at 35^{o}C. The vapor activity was controlled automatically by mixing the wet C_2H_5OH vapor feed with a dry N_2 line. As such, N_2 serves as a carrier gas for the vapors. The samples "dry mass" was measured under N_2 and were at equilibrium with N_2 before introduction of the vapors to the sample chamber. A large N_2 purge flow rate is used to minimize heat and mass transfer effects.

The kinetic uptake data of C_2H_5OH on the 162 μm ZIF-8 sample were analyzed to obtain the corrected diffusivity. Due to the difference in experimental techniques, the C_2H_5OH diffusivity determination requires special attention. In this experiment, the vapors were substantially below their vapor pressure and were carried by N_2 sweep gas past a small pan bearing a single layer of ZIF-8 crystals. As such, estimates of the mass transfer coefficient are appropriate in order to ensure that intracrystalline diffusion is the limiting factor. Accounting for an effective mass transfer coefficient (k_m) through a totally stagnant gas filled pan with depth (δ) of 0.1 cm and a gas phase diffusion coefficient (D_g) ~ 0.1 cm^2/s, the effective mass transfer coefficient $k_m = D_g / \delta = 1$ cm/s. The ratio of the external resistance to the internal diffusion resistance can be seen[18], viz.,

$$\lambda = \frac{R \times k_m}{D_{ZIF-8}} \tag{16}$$

where R (cm) is the radius of ZIF-8 crystal, $D_{ZIF\text{-}8}$ (cm^2/s) is the diffusivity of C_2H_5OH in ZIF-8. Finally, a reasonable estimate for an internally controlled system is an order of magnitude difference between external and internal resistances ($\lambda > 10$)[18]. In order to have $\lambda \leq 10$, the vapor diffusivity would need to be no smaller than 10^{-3} cm^2/s for the 162 μm ZIF-8 sample. As even the fastest diffusing gas

studied (Helium) has a diffusion coefficient around 10^{-3} cm^2/s, and it is logical to assume that C_2H_5OH will diffuse slower than Helium, it is reasonable to conclude that the vapor diffusion into the samples is internally limited. Thus, the analysis presented in the preceding section for determining the diffusion coefficient is valid for this experimental system as well.

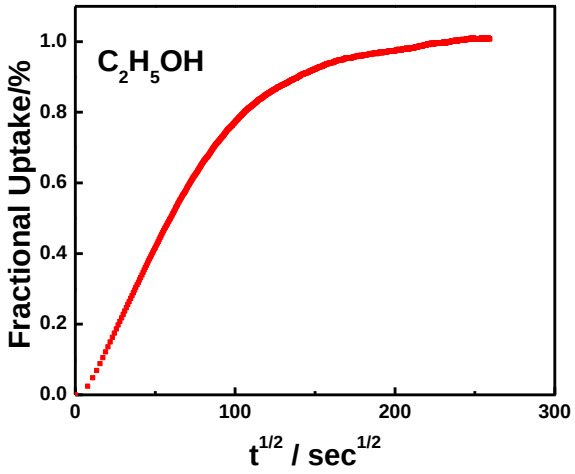

Figure S7. Kinetic uptake of C_2H_5OH in the 162 μm synthesized ZIF-8 sample at 35 ℃ (p/p_0=0.08).

The corrected diffusivity of C_2H_5OH (1.4×10^{-9} cm^2/s, Table S3) was obtained by analyzing the C_2H_5OH uptake curve in the 162 μm synthesized ZIF-8 sample (Figure S8) at p/p_0=0.08. Unlike the case of pressure decay method, the vapor-phase concentration during the uptake was essentially constant for the gravimetric method. Hence, Equation S9 instead of S13 was chosen to derive theoretical uptake curve. Similar to analysis of gas kinetic uptake data, effective diffusivity of C_2H_5OH in ZIF-8 was obtained by matching the initial region ($0<M_t/M_\infty<0.2$) of the experimental uptake curve (Figure S7) with equation S9. The value of D/D_0 was assumed to be unity, since the adsorption isotherm was essentially linear at p/p_0=0.08.

Section S4: Calculation of diffusivities from mixed matrix membrane permeation results

Details regarding fabrication and characterization (SEM images, TGA curves, C_3H_6 and C_3H_8 permeation results) of 6FDA-DAM neat dense films and ZIF-8/6FDA-DAM mixed matrix dense films can be found in our previous work[23]. The ~200nm BASF ZIF-8 crystals that were used to fabricate ZIF-8/6FDA-DAM mixed matrix membranes were shown in Figure 1 (a). Table S4 shows He, H_2, CO_2, O_2, N_2, CH_4, C_2H_4, and C_2H_6 pure component permeation results of neat 6FDA-DAM dense films and ZIF-8/6FDA-DAM mixed matrix dense films with 23.8 vol% ZIF-8 loading at 35℃ and 2 bar upstream pressure (pressure in the downstream was negligible). Pure component permeabilities of all the penetrants with the exception of H_2 were the average of two films at each particle loading (Table S5). The permeabilities of H_2 were from single films at each loading, and therefore no uncertainty information was available for this penetrant.

Table S4. Pure component permeabilities of the neat 6FDA-DAM dense films and ZIF-8/6FDA-DAM mixed matrix dense films at 35 ℃.

	ZIF-8 loading (vol %)	P_{He} (Barrer*)	P_{H2} (Barrer)	P_{CO2} (Barrer)	P_{O2} (Barrer)	P_{N2} (Barrer)	P_{CH4} (Barrer)	P_{C2H4} (Barrer)	P_{C2H6} (Barrer)
6FDA-DAM	0	339±17	483	512±25	103±5	27.9±2.5	22.6±2.1	39.4±1.5	12.0±0.2
ZIF-8/6FDA-DAM	23.8	621±5	899	781±3	186±4	48.5±0.6	41.2±0.5	72.9±2.5	22.8±0.8

*1 Barrer = [10^{-10} cm^3(STP) cm/(cm^2 s cmHg)]

Table S5. Pure component permselectivities of the neat 6FDA-DAM dense films and ZIF-8/6FDA-DAM mixed matrix dense films at 35 ℃.

	ZIF-8 loading (vol %)	α (CO_2/N_2)	α (CO_2/CH_4)	α (O_2/N_2)	α (H_2/CH_4)	α (H_2/N_2)	α (H_2/C_3H_8)	α (C_2H_4/C_2H_6)
6FDA-DAM	0	18.3±0.9	22.6±0.9	3.9±0.4	21.4±0.6	17.3±1.7	380±16	3.3±0.2
ZIF-8/6FDA-DAM	23.8	16.1±0.3	19.0±0.3	4.0±0.1	21.8±0.3	18.5±0.3	612±59	3.2±0.2

Permeability of He, H_2, CO_2, O_2, N_2, CH_4, C_2H_4, C_2H_6, C_3H_6 and C_3H_8 in the pure ZIF-8 phase (Table S6) was back-calculated using the pure gas permeation data of neat 6FDA-DAM dense films and ZIF-8/6FDA-DAM mixed matrix dense films with 23.8 vol% ZIF-8 loading (referred to as DAMZ_1 in

our previous work[23]) by the Maxwell model, which is the most widely employed model to predict permeability of composite materials[24]:

$$P_{MMM} = P_p \left[\frac{P_s + 2P_p - 2\Phi_s(P_p - P_s)}{P_s + 2P_p + \Phi_s(P_p - P_s)} \right] \quad (17)$$

where P_{MMM} [10^{-10}cm^3(STP) cm/(cm^2 s cmHg)] is permeability in the mixed matrix ZIF-8/6FDA-DAM dense film; P_p is permeability in the neat 6FDA-DAM dense film; P_s is permeability in dispersed ZIF-8 particles; and Φ_s is volume fraction of ZIF-8 in the mixed matrix ZIF-8/6FDA-DAM dense film. The validity of employing the Maxwell model to back-calculate permeability in dispersed molecular sieve particles depends on (1) the molecular sieve particles adhering well with the polymer matrix (2) the volume percentage of molecular sieve particles in the polymer being low and can be unambiguously determined and (3) the molecular sieve particles are well-dispersed. As shown in our previous work[23], excellent adhesion was achieved between ZIF-8 particles and the 6FDA-DAM matrix at all ZIF-8 loadings. Also, the ZIF-8 volume fraction of the film (23.8 vol. %) used for permeability calculation was sufficiently low and determined quantitatively by TGA. So we believe that the assumptions of the Maxwell model were essentially satisfied for our calculations. The uncertainties in experimental permeabilities of the dense films (Table S4) were taken into account for calculation of permeabilities (average of physically possible numbers) in the pure ZIF-8 phase (Table S6). In our previous study[23], permeabilities of C_3H_6 and C_3H_8 in the pure ZIF-8 phase were based on average dense films permeabilities.

The corrected diffusivity (Table S6) in dispersed ZIF-8 particles can be further obtained from permeability in dispersed ZIF-8 particles using the following relationship suggested by Koros[25]:

$$P = \tilde{D} \times \tilde{S} \quad (18)$$

$$\tilde{D} = \left[\int_{C_1}^{C_2} D(C)\, dC \right] \Big/ \left[\int_{C_1}^{C_2} dC \right] \quad (19)$$

$$\tilde{S} = (C_2 - C_1) / (p_2 - p_1) \quad (20)$$

where $\tilde{D}$ (cm^2/s) and $\tilde{S}$ ($cm^3[STP] \cdot cm^{-3} \cdot bar^{-1}$) are average effective transport diffusivity and adsorption coefficient in dispersed ZIF-8 particles, C_1 (mmol/g) and C_2 (mmol/g) are the penetrant (adsorbate) concentrations in the ZIF-8 particles at the downstream and upstream side of the membrane, p_1 (bar) and p_2 (bar) are penetrant (adsorbate) pressure in the downstream and upstream side of the membrane. To calculate the corrected diffusivities of He, H_2, CO_2, O_2 N_2, and CH_4 whose adsorption isotherms can be described by Henry's law (Equation S3) in the pressure range of permeation measurements (≤ 2 bar), the following may be used:

$$P = \tilde{D} \times \tilde{S} = D_0 C_s b = D_0 K \tag{21}$$

To calculate the corrected transport diffusivity of C_2H_4, C_2H_6, C_3H_6 and C_3H_8, whose adsorption isotherms can be described by the Langmuir adsorption isotherm (Equation S2) in the pressure range of permeation measurements (≤ 2 bar), the following may be used:

$$P = \tilde{D} \times \tilde{S} = \frac{D_0 C_s}{p_2 - p_1} \ln \frac{C_s - C_1}{C_s - C_2} = \frac{D_0 C_s}{p_2 - p_1} \ln(\frac{1 + bp_2}{1 + bp_1}) \tag{22}$$

During the permeation measurements, the downstream pressure was negligible compared with the upstream pressure, therefore Equation S22 can be simplified to:

$$P = \tilde{D} \times \tilde{S} = \frac{D_0 C_s}{p_2} \ln \frac{C_s}{C_s - C_2} = \frac{D_0 C_s}{p_2} \ln(1 + bp_2) \tag{23}$$

Table S6. Permeabilitites and corrected diffusivities in the pure ZIF-8 phase at 35 ℃.

	He	H_2	CO_2	O_2	N_2	CH_4	C_2H_4	C_2H_6	C_3H_6	C_3H_8
P (Barrer)	$2.7 \pm 2.2 \times 10^4$	2.2×10^4	$3.3 \pm 0.8 \times 10^3$	$2.5 \pm 1.3 \times 10^3$	$1.0 \pm 0.8 \times 10^3$	270 ± 26	$1.1 \pm 0.5 \times 10^3$	430 ± 130	210 ± 95	2.5 ± 1.1
D_0 (cm^2/s)	$6.5 \pm 5.2 \times 10^{-4}$	2.0×10^{-4}	$2.1 \pm 0.5 \times 10^{-6}$	$1.0 \pm 0.5 \times 10^{-5}$	$4.0 \pm 3.0 \times 10^{-6}$	$4.0 \pm 0.4 \times 10^{-7}$	$3.6 \pm 1.6 \times 10^{-7}$	$8.8 \pm 2.7 \times 10^{-8}$	$1.6 \pm 0.3 \times 10^{-8}$	$1.7 \pm 0.8 \times 10^{-10}$

As suggested by Table S6, for the pure ZIF-8 phase, the permselectivity of CO_2/CH_4 and CO_2/N_2 were both lower than that of neat 6FDA-DAM polymer (see Table S5). The pure component permselectivities of H_2/C_3H_8 were significantly higher than the reported separation factors of a pure ZIF-8 membrane grown above a porous α-alumina support, which were measured in a mixed-gas feed

environment[26]. While competitive adsorption and diffusion in mixed-gas environmental contribute to the discrepancies somewhat, it is possible that even very small defects in the pure ZIF-8 membrane could lead to separation factors that are significantly lower than the intrinsic values. Due to uncertainties in measurements of dense film permeabilities, the resulting uncertainties in permeabilities and diffusivities in the pure ZIF-8 phase as shown in Table S6 were large, however, were reliable on their order of magnitude.

The estimated effective aperture size for molecular sieving (4.0-4.2Å) is generally confirmed by the membrane permeation results. For penetrants that are not larger than this effective size range (i.e. He, H_2, CO_2, O_2, N_2, CH_4, C_2H_4 and C_2H_6), ZIF-8 is not particularly selective and two component permselectivities cannot be enhanced by incorporating ZIF-8 particles in the 6FDA-DAM polymer matrix. As long as one penetrant (H_2/C_3H_8) or both penetrants (C_3H_6/C_3H_8) become larger than this effective size range, ZIF-8 become fairly size selective and the membrane permselectivity can be enhanced.

Bux and co-workers[27,28] reported transport diffusivity of CO_2 (~1.5×10^{-6} cm^2/s), CH_4 (~1.0×10^{-6} cm^2/s), C_2H_4 (~5×10^{-7} cm^2/s), and C_2H_6 (~1×10^{-7} cm^2/s) in ZIF-8 at low concentrations using the IR-Microscopy method, which were respectively on the same order of magnitude to the corrected diffusivities shown in Table S6. Pantatosaki and co-workers[29] reported self-diffusivity of CO_2 and CH_4 in ZIF-8 at higher concentrations determined by the PFG-NMR technique, which were both in the range of 1~2×10^{-6} cm^2/s. These suggest that *if the assumptions of the Maxwell model can be satisfied*, mixed membrane permeation could be an approach with order of magnitude reliability to obtain transport diffusivity in the dispersed molecular sieving phase. It is necessary to mention that the IR-Microscopy and PFG-NMR measurements were done at a slightly lower temperature (~300 K). We believe that a justification of comparison could be made since the effect of 10 K temperature difference on the diffusivities should be trivial considering that the diffusional activation energies for these fast diffusing gases are expected to be low.

Section S5: Estimation of molecular diameters

In order to estimate the effective molecular sieving aperture size of ZIF-8, it is essential to have knowledge of the dimension of probe molecules. A variety of scales have been used to characterize molecular dimensions [8,30,31] (e.g. kinetic diameter, van der Waals diameter, Lennard-Jones diameter, and critical molecular diameter). Unfortunately, none of these scales is capable of satisfactorily characterizing molecular dimensions with respect to the relative diffusion rates for all the studied penetrants.

The scale of kinetic diameters by Breck[30] was adopted for this study with a few modifications. This scale, which was based on the minimum equilibrium cross-sectional diameters, was capable of explaining the molecular sieving behavior of zeolites for simple diffusing molecules[30] (e.g. adsorption of CO_2 with exclusion of N_2 on zeolite 3A) as well as linear and branched paraffins (e.g. adsorption of n-C_4H_{10} with exclusion of iso-C_4H_{10} on zeolite 5A). However, according to Breck[30], the kinetic diameters of linear paraffin C_3H_8 and n-C_4H_{10} (both listed as ~ 4.3 Å) are smaller than those of linear olefins C_3H_6 and 1-C_4H_8 (both listed as ~ 4.5 Å). This has been shown to be questionable on the basis of faster diffusion of linear olefins than the corresponding linear paraffins in both microporous molecular sieves and polymers[13,31-33]. On the other hand, the scale of van der Waals diameter suggested by Ruthven[7] was able to reflect the subtle size differences of linear olefin/paraffin molecules (C_3H_6/C_3H_8 and 1-C_4H_8/n-C_4H_{10}) , which is given in equation S24.

$$b = \frac{4}{3}\pi\left(\frac{\sigma_0}{2}\right)^3 \times 4 \qquad (24)$$

where σ_0 (Å) is the van der Waals diameter[8], b (Å^3) is the van der Waals co-volume, which can be calculated from fluid critical parameters[7]. Moreover, the van der Waals diameter was used for C_2H_5OH, since no kinetic diameter data were provided for this penetrant.

Ruthven correlated diffusional activation energies in zeolite LTA and carbon molecular sieves with van der Waals diameters for simple molecules as well as linear hydrocarbons[8]. In our study,

however, the scale of van der Waals diameter was not adopted for all the penetrants. N_2 is smaller than CO_2 in the scale of van der Waals diameters (Table S7). However, as mentioned before, CO_2 can adsorb on zeolite 3A but N_2 is excluded. Another limitation of this scale is that it cannot explain slower diffusion of iso-C_4H_{10} than n-C_4H_{10} in many systems[13,34]. Therefore, we believe that a hybrid molecular dimension scale based on kinetic diameter and the van der Waals diameter will be most appropriate for our study.

Table S7. Estimated molecular diameters for the studied probe molecules.

	Kinetic diameter[30] (Å)	van der Waals diameter (Å)
He	2.6	2.66
H_2	2.89	2.76
CO_2	3.3	3.24
O_2	3.46	2.94
N_2	3.64	3.13
CH_4	3.8	3.25
C_2H_4	3.9	3.59
C_2H_6	N/A	3.72
C_3H_6	4.5	4.03
C_3H_8	4.3	4.16
1-C_4H_8	4.5	4.41
n-C_4H_{10}	4.3	4.52
iso-C_4H_8	4.8	4.42
iso-C_4H_{10}	5.0	4.52
C_2H_5OH	N/A	4.10

Section S6. Evaluation of ZIF-8 as an adsorbent and membrane material for hydrocarbon separations

Based on the adsorption and permeation results obtained in previous sections, we further evaluated the potential of using ZIF-8 as an adsorbent and membrane material for separation of binary hydrocarbon mixtures, i.e. C_3H_6/C_3H_8, 1-C_4H_8/n-C_4H_{10}, iso-C_4H_8/iso-C_4H_{10}, and n-C_4H_{10}/iso-C_4H_{10}.

Hydrocarbon separations are the most significant separations in the petrochemical industry. The low-molecular weight olefins and iso-paraffins are essential ingredients to the alkylation process for production of premium motor fuels with high-octane values[35,36]. On the other hand, the low-molecular olefins are feedstocks for the manufacturing of a variety of important chemicals such as polyethylene, polypropylene, polybutylene, polybutadiene, butylene oxide, methy ethyl ketone, and methyl tertiary butyl ether (MTBE), etc.

Adsorptive separation can be achieved on the basis of equilibrium selectivity or kinetic selectivity[9]. For a pressure swing adsorption (PSA) system operating at linear conditions (linear driving force assumption), the equilibrium selectivity is given by[37]:

$$\alpha_e = K_1 / K_2 \tag{25}$$

where α_e is the equilibrium selectivity, K_1 and K_2 are Henry's constants of the more and less strongly adsorbed species. Like non-cationic zeolites[37] but unlike cationic zeolites and a recently reported large pore (~11 Å) metal-organic framework Fe_2(dobdc)[38], paraffins adsorb slightly stronger than corresponding olefins in ZIF-8 with equilibrium selectivities less than two (Table S8). Therefore, ZIF-8 will not be an attractive adsorbent for olefin/paraffin mixtures based on equilibrium selectivity. Nonetheless, the molecular sieving nature of ZIF-8 make it a potential candidate for kinetic separations, in which separation of a gas mixture by passing through an adsorbent bed is achieved based on the difference in diffusion rates rather than adsorption strength. For convenience, the diffusion selectivity can be used to access the utility of ZIF-8 for such kinetic separation:

$$\alpha_D = D_1 / D_2 \tag{26}$$

where D_1 and D_2 (cm^2/s) are diffusivities of the faster and slower diffusing species.

For separation of butane isomers (n-C_4H_{10}/iso-C_4H_{10}), the slower and less adsorbed iso-C_4H_{10} is the desired product. Enrichment of iso-C_4H_{10} in the raffinate could be efficiently achieved on a ZIF-8 adsorbent bed thanks to large differences in diffusion rates of n-C_4H_{10} and iso-C_4H_{10}. For olefin/paraffin separations (i.e. C_3H_6/C_3H_8, 1-C_4H_8/n-C_4H_{10}, and iso-C_4H_8/iso-C_4H_{10}), however, the faster and more adsorbed olefin is the desired product, which has to be recovered as desorbate streams from the ZIF-8 adsorbent bed by applying temperature swing or displacement desorption process[37]. Since paraffins adsorb in ZIF-8 simultaneously, the purity of olefins in the desorbate stream is dependent not only on the relative diffusion rate of olefin/paraffin, but also on their relative adsorption strength[37]:

$$s = \frac{K_O}{K_P}\sqrt{\frac{D_O}{D_P}} = \frac{1}{\alpha_e}\sqrt{\alpha_D} \tag{27}$$

$$Y = \frac{s}{1+s} \times 100\% \tag{28}$$

where s is the separation factor, Y (%) is the purity of olefins in the desorbate stream, α_D is the effective diffusion selectivity, K_O and K_P (mmol/g/bar) are Henry's constants of olefin and paraffin, D_O and D_P (cm^2/s) are diffusivity of olefin and paraffin. The square root dependence on α_D appears due to the transient uptake relationship in a time varying PSA process[37]. Since paraffin is the more strongly adsorbed species on ZIF-8, K_O/K_P is equal to $1/\alpha_e$ and smaller than unity. This suggests that in a PSA process, the effective diffusion selectivity of olefin/paraffin on ZIF-8 is offset by the stronger adsorbed paraffins. Table S8 shows that in a PSA process, as a kinetically selective adsorbent, ZIF-8 is ideally capable of enriching 90% C_3H_6 and 90% iso-C_4H_8 streams from binary mixtures of C_3H_6/C_3H_8 and iso-C_4H_8/iso-C_4H_{10}, respectively. While the diffusion rate of C_3H_6 is 2~4 orders of magnitude higher, ZIF-8 as a kinetically selective adsorbent is not competitive with small pore eight-ring zeolite (zeolite 4A,

AlPO-14, SiCHA and DD3R) in terms of the highest product purity, in which desorbate streams with 99% C_3H_6 purity were expected[37,39].

Table S8. Evaluation of ZIF-8 as kinetically selective adsorbent for olefin/paraffin separations.

	α_e	α_D	s	Y /%
C_3H_6/C_3H_8	1.3	140*	9.1	90%
1-C_4H_8/n-C_4H_{10}	1.0	2.3	1.5	60%
iso-C_4H_8/iso-C_4H_{10}	1.5	180	8.9	90%

*Calculated using diffusivity obtained from kinetic uptake measurements.

On the other hand, our analysis shows that efficient separation of hydrocarbon mixtures could be realized by membranes fabricated with ZIF-8. Table S9 shows the pure component permeability of C_3 and C_4 hydrocarbons on a pure ZIF-8 membrane operated at 35 ℃ and 2 bars upstream pressure (vacuum in the downstream). The permeability of C_3 and C_4 hydrocarbons were calculated from the equilibrium and kinetic adsorption results in Section S3 using equation S23. For separation of C_3H_6/C_3H_8 and iso-C_4H_8/iso-C_4H_{10}, a membrane is obviously the more favorable option over adsorption in terms of product purity. The estimated pure component permselectivity of C_3H_6/C_3H_8 and iso-C_4H_8/iso-C_4H_{10} on a pure ZIF-8 membrane were 130 and 180, respectively, which are promising to enrich permeate with to high olefin purities. However, for separation of iso-C_4H_8/iso-C_4H_{10}, the permeability of iso-C_4H_8 was so low that an unreasonably thin ZIF-8 layer would have to be fabricated to achieve a practical productivity.

Figure 5 shows the permeability of all the studied penetrant versus molecular diameters. According to Figure 3, the larger and slower diffusing molecules always show higher adsorption coefficients in ZIF-8, therefore the kinetic selectivities in ZIF-8 are generally offset by the equilibrium selectivities, resulting in permselectivities that are generally lower than the kinetic selectivities.

The potential of using ZIF-8 as a membrane material for separation of C_3H_6/C_3H_8 mixtures was again compared with that of small pore (~3.8 Å) eight ring zeolites (zeolite 4A, AlPO-14, SAPO-34, SiCHA, and DD3R), whose apertures are relatively rigid. While the C_3H_6/C_3H_8 kinetic selectivity (10^4 ~ infinity) of these rigid molecular sieves are much higher than that of ZIF-8 with flexible structure (kinetic selectivity of 140 as suggested by Table S3), the diffusion rates of C_3H_6 in these small pore zeolites are 10^2 ~ 10^4 slower[37,39,40]. Therefore, ZIF-8 is obviously the preferred membrane material in terms of overall process economics since theoretically a C_3H_6/C_3H_8 permselectivity over 35 is high enough to de-bottleneck the fractional distillation unit (C_3 splitter) for large-scale C_3H_6/C_3H_8 separations[41].

We would like to mention that the above analysis was based on pure component adsorption and permeation measurements. In realistic conditions with mixture feeds, the mobility of faster diffusing component might be reduced, which may result in a decreased kinetic selectivity and permselectivity.

Table S9. Calculated pure component permeability on a pure ZIF-8 membrane operated at 35 ℃ and 2 bars upstream pressure.

	Permeability [10^{-10} cm^3(STP) cm/(cm^2 s cmHg)]
C_3H_6	390*
C_3H_8	2.9*
1-C_4H_8	0.30
n-C_4H_{10}	0.12
iso-C_4H_8	8.8E-6
iso-C_4H_{10}	5.0E-8

*Calculated using diffusivity obtained from kinetic uptake measurements.

Table S10. Calculated ideal permselectivities on a pure ZIF-8 membrane operated at 35 ℃ and 2 bars upstream pressure, based on the results in Table S9.

	Permselectivity
C_3H_6/C_3H_8	130*
1-C_4H_8/n-C_4H_{10}	2.5
iso-C_4H_8/iso-C_4H_{10}	180
n-C_4H_8/iso-C_4H_{10}	2.4×10^6

*Calculated using diffusivity obtained from kinetic uptake measurements.

Testing permeation properties of a pure molecular sieving membrane with probe penetrants could be used to study its molecular sieving properties, as long as differences in adsorption capacities of the penetrants can be taken into account. This approach, however, works less well for large penetrants with very slow permeation rates. Due to intrinsic limitations of permeation tests (system leaking rate, gas chromatography sensitivity, etc.) and/or membrane defects, it is impractical to unbiasedly determine the actual permeation flux of these slowly diffusing penetrants. Tomita and co-workers[42] reported pure gas permeances of zeolite DDR membrane that was formed on a porous alumina substrate. The reported "permeance-kinetic diameter" curve flattened out for n-C_4H_{10}, iso-C_4H_{10}, and SF_6, which may potentially be attributed to few defects on the membrane. Similarly, Pan and co-workers[43] reported C_3H_6/C_3H_8 permselectivity of ~15 and almost identical permeances of n-C_4H_{10} and iso-C_4H_{10} on a ZIF-8/α-alumina composite membrane, which were inconsistent with the values that we obtained from kinetic uptake measurements (Table S10). These inconsistencies were probably due to the defective nature of the pure ZIF-8 layer, which was confirmed by their later work reporting much higher C_3H_6/C_3H_8 permselectivities[44]. Unfortunately, permeation results of C_4 hydrocarbons were not reported in their later work.

References

(1) Cravillon, J.; Munzer, S.; Lohmeier, S.-J.; Feldhoff, A.; Huber, K.; Wiebcke, M. Rapid Room-Temperature Synthesis and Characterization of Nanocrystals of a Prototypical Zeolitic Imidazolate Framework. *Chem. Mater.* **2009**, *21*, 1410-1412.

(2) Cravillon, J.; Schröder, C. A.; Bux, H.; Rothkirch, A.; Caro, J.; Wiebcke, M. Formate modulated solvothermal synthesis of ZIF-8 investigated using time-resolved in situ X-ray diffraction and scanning electron microscopy. *CrystEngComm* **2012**, *14*, 492.

(3) Park, K. S.; Ni, Z.; Cote, A. P.; Choi, J. Y.; Huang, R.; Uribe-Romo, F. J.; Chae, H. K.; O'Keeffe, M.; Yaghi, O. M. Exceptional chemical and thermal stability of zeolitic imidazolate frameworks. *Proc. Natl. Acad. Sci. U. S. A.* **2006**, *103*, 10186-10191.

(4) Llewellyn, P. L.; Coulomb, J. P.; Grillet, Y.; Patarin, J.; Andre, G.; Rouquerol, J. Adsorption by MFI-type zeolites examined by isothermal microcalorimetry and neutron diffraction. 2. Nitrogen and carbon monoxide. *Langmuir* **1993**, *9*, 1852-1856.

(5) Fairen-Jimenez, D.; Moggach, S. A.; Wharmby, M. T.; Wright, P. A.; Parsons, S.; Duren, T. Opening the Gate: Framework Flexibility in ZIF-8 Explored by Experiments and Simulations. *J. Am. Chem. Soc.* **2011**, *133*, 8900-8902.

(6) Zimmerman, C. M.; Singh, A.; Koros, W. J. Diffusion in gas separation membrane materials: A comparison and analysis of experimental characterization techniques. *J. Polym. Sci. Pt. B-Polym. Phys.* **1998**, *36*, 1747-1755.

(7) Lide, D. R. *Handbook of Chemistry and Physics, 87th Edition*; CRC Press, LLC, 2006.

(8) Ruthven, D. M.: *Principles of Adsorption and Adsorption Processes*; John Wiley & Sons, Inc., 1984.

(9) Yang, R. T. *Adsorbents: Fundamentals and Applications*; John Wiley & Sons, Inc., 2003.

(10) Prausnitz, J. M.; Lichtenthaler, N.; Azevedo, E. G. D. *Molecular Thermodynamics of Fluid-Phase Equilibria (3rd Edition)*; Prentice Hall, 1998.

(11) Lively, R. P.; Dose, M. E.; Thompson, J. A.; McCool, B. A.; Chance, R. R.; Koros, W. J. Ethanol and water adsorption in methanol-derived ZIF-71. *Chem. Commun.* **2011**, *47*, 8667-8669.

(12) Nalaparaju, A.; Zhao, X. S.; Jiang, J. W. Molecular Understanding for the Adsorption of Water and Alcohols in Hydrophilic and Hydrophobic Zeolitic Metal–Organic Frameworks. *J. Phys. Chem. C* **2010**, *114*, 11542-11550.

(13) Karger, J.; Ruthven, D. M. *Diffusion in Zeolites and Other Microporous Solids.*; John Wiley & Sons, Inc., 1991.

(14) Karge, H. G.; Weitkamp, J. *Adsorption and Diffusion*; Springer-Verlag Berlin Heidelberg, 2008.

(15) Keil, F. J.; Krishna, R.; Coppens, M. O. Modeling of diffusion in zeolites. *Rev. Chem. Eng.* **2000**, *16*, 71-197.

(16) Ruthven, D. M.; Loughlin, K. F. The effect of crystallite shape and size distribution on diffusion measurements in molecular sieves. *Chem. Eng. Sci.* **1971**, *26*, 577-584.

(17) Ruthven, D. M. Sorption kinetics for diffusion-controlled systems with a strongly concentration-dependent diffusivity. *Chem. Eng. Sci.* **2004**, *59*, 4531-4545.

(18) Crank, J. *The Mathematics of Diffusion*; Oxford University Press Inc., 1975.

(19) Yucel, H.; Ruthven, D. M. DIFFUSION IN 5A-ZEOLITE - STUDY OF THE EFFECT OF CRYSTAL SIZE. *J. Chem. Soc., Faraday Trans.* **1980**, *76*, 71-83.

(20) Berens, A. R. Diffusion and relaxation in glassy polymer powders: 1. Fickian diffusion of vinyl chloride in poly(vinyl choride). *Polymer* **1977**, *18*, 697-704.

(21) Berens, A. R.; Hopfenberg, H. B. Diffusion and relaxation in glassy polymer powders: 2. Separation of diffusion and relaxation parameters. *Polymer* **1978**, *19*, 489-496.

(22) Enscore, D. J.; Hopfenberg, H. B.; Stannett, V. T. Effect of particle size on the mechanism controlling n-hexane sorption in glassy polystyrene microspheres. *Polymer* **1977**, *18*, 793-800.

(23) Zhang, C.; Dai, Y.; Johnson, J. R.; Karvan, O.; Koros, W. J. High performance ZIF-8/6FDA-DAM mixed matrix membrane for propylene/propane separations. *J. Membr. Sci.* **2012**, *389*, 34-42.

(24) Moore, T. T.; Mahajan, R.; Vu, D. Q.; Koros, W. J. Hybrid membrane materials comprising organic polymers with rigid dispersed phases. *AIChE J.* **2004**, *50*, 311-321.

(25) Koros, W. J.; Fleming, G. K.; Jordan, S. M.; Kim, T. H.; Hoehn, H. H. Polymeric membrane materials for solution-diffusion based permeation separations. *Prog. Polym. Sci.* **1988**, *13*, 339-401.

(26) Bux, H.; Feldhoff, A.; Cravillon, J.; Wiebcke, M.; Li, Y.-S.; Caro, J. Oriented Zeolitic Imidazolate Framework-8 Membrane with Sharp H2/C3H8 Molecular Sieve Separation. *Chem. Mater.* **2011**, *23*, 2262-2269.

(27) Bux, H.; Chmelik, C.; van Baten, J. M.; Krishna, R.; Caro, J. Novel MOF-Membrane for Molecular Sieving Predicted by IR-Diffusion Studies and Molecular Modeling. *Adv. Mater.* **2010**, *22*, 4741-4743.
(28) Bux, H.; Chmelik, C.; Krishna, R.; Caro, J. Ethene/ethane separation by the MOF membrane ZIF-8: Molecular correlation of permeation, adsorption, diffusion. *J. Membr. Sci.* **2011**, *369*, 284-289.
(29) Pantatosaki, E.; Megariotis, G.; Pusch, A.-K.; Chmelik, C.; Stallmach, F.; Papadopoulos, G. K. On the Impact of Sorbent Mobility on the Sorbed Phase Equilibria and Dynamics: A Study of Methane and Carbon Dioxide within the Zeolite Imidazolate Framework-8. *J. Phys. Chem. C* **2011**, *116*, 201-207.
(30) Breck, D. W. *Zeolite Molecular Sieves*; Robert E. Krieger Publishing Company, INC., 1973.
(31) Yampolskii, Y.; Pinnau, I.; Freeman, B. D. *Materials Science of Membranes*; John Wiley & Sons Ltd, 2006.
(32) Xu, L. R.; Rungta, M.; Koros, W. J.: Matrimid (R) derived carbon molecular sieve hollow fiber membranes for ethylene/ethane separation. *J. Membr. Sci.* **2011**, *380*, 138-147.
(33) Rungta, M.; Xu, L. R.; Koros, W. J. Carbon molecular sieve dense film membranes derived from Matrimid (R) for ethylene/ethane separation. *Carbon* **2012**, *50*, 1488-1502.
(34) Esekhile, O.; Qiu, W.; Koros, W. J. Permeation of butane isomers through 6FDA-DAM dense films. *J. Polym. Sci., Part B: Polym. Phys.* **2011**, *49*, 1605-1620.
(35) Gary, J. H.; Handwerk, G. E. *Petroleum Refinning Technology and Economics*; MARCEL DEKKER, INC., 1975.
(36) Liu, J.; Bae, T.-H.; Qiu, W.; Husain, S.; Nair, S.; Jones, C. W.; Chance, R. R.; Koros, W. J. Butane isomer transport properties of 6FDA–DAM and MFI–6FDA–DAM mixed matrix membranes. *J. Membr. Sci.* **2009**, *343*, 157-163.
(37) Ruthven, D. M.; Reyes, S. C. Adsorptive separation of light olefins from paraffins. *Microporous Mesoporous Mat.* **2007**, *104*, 59-66.
(38) Bloch, E. D.; Queen, W. L.; Krishna, R.; Zadrozny, J. M.; Brown, C. M.; Long, J. R. Hydrocarbon Separations in a Metal-Organic Framework with Open Iron(II) Coordination Sites. *Science* **2012**, *335*, 1606-1610.
(39) Padin, J.; Rege, S. U.; Yang, R. T.; Cheng, L. S. Molecular sieve sorbents for kinetic separation of propane/propylene. *Chem. Eng. Sci.* **2000**, *55*, 4525-4535.
(40) Agarwal, K.; John, M.; Pai, S.; Newalkar, B. L.; Bhargava, R.; Choudary, N. V. SAPO-34 assisted C_3 separation: Modeling and simulation. *Microporous Mesoporous Mat.* **2010**, *132*, 311-318.
(41) Colling, C. W.; Huff Jr, G. A.; Bartels, J. V. *US Patent*, 2004.
(42) Tomita, T.; Nakayama, K.; Sakai, H. Gas separation characteristics of DDR type zeolite membrane. *Microporous Mesoporous Mat.* **2004**, *68*, 71-75.
(43) Pan, Y.; Lai, Z. Sharp separation of C_2/C_3 hydrocarbon mixtures by zeolitic imidazolate framework-8 (ZIF-8) membranes synthesized in aqueous solutions. *Chem. Commun.* **2011**, *47*, 10275.
(44) Pan, Y.; Li, T.; Lestari, G.; Lai, Z. Effective separation of propylene/propane binary mixtures by ZIF-8 membranes. *J. Membr. Sci.* **2012**, *390-391*, 93-98.